Cooperative control of multiple surface vessels with discrete-time periodic communications

J. Almeida*,†, C. Silvestre and A. M. Pascoal

Institute for Systems and Robotics, Instituto Superior Técnico, Av. Rovisco Pais, 1049-001 Lisboa, Portugal

SUMMARY

This paper addresses the problem of cooperative path-following of networked autonomous surface vessels with discrete-time periodic communications. The objective is to steer a group of autonomous vehicles along given spatial paths, while holding a desired inter-vehicle formation pattern. For a given class of marine vessels, we show how Lyapunov based techniques, graph theory, and results from networked control systems can be brought together to yield a decentralized control structure where the dynamics of the cooperating vessels and the constraints imposed by the topology of the inter-vehicle communication network are explicitly taken into account. Cooperation is achieved by adjusting the speed of each vessel along its path according to information exchanged periodically on the positions of a subset of the other vessels, as determined by the communications topology adopted. The closed loop system that is obtained by putting together the path-following and cooperation strategies takes an interconnected feedback form where both systems are input-to-state stable (ISS) with respect to the outputs of each other. Using a small-gain theorem, stability and convergence of the overall system are guaranteed for adequate choices of the controller gains.

KEY WORDS: cooperative motion control; path-following; autonomous surface vessels; nonlinear adaptive control; graph theory.

1. INTRODUCTION

There has been growing interest in the development of multiple vehicles for a number of scientific and commercial mission scenarios. Among a myriad of applications related to multi-agent systems involving autonomous or unmanned vehicles, we point out the use of unmanned aerial vehicles (UAVs) for fire detection in forests, autonomous underwater vehicles (AUVs) for seabed surveying and environmental monitoring, and groups of autonomous surface vessels (ASVs) for data acquisition at sea or to serve as mobile baseline systems for underwater target positioning [1]. In all scenarios, cooperation among the vehicles is essential in order to accomplish mission goals in an efficient and robust manner. In most cases, cooperation is achieved through the exchange of information among vehicles, implying that control mechanisms must be designed taking into account such practical constraints as limited bandwidth and intermittent communication failures.

1.1. Surface vessels as ocean observation tools

Among the different types of autonomous marine vehicles, ASVs are becoming increasingly important in view of their simplicity of construction and the potential to sample the ocean

This is a pre-print version of the following article:
Almeida, J., Silvestre, C. and Pascoal, A. M. (2011), Cooperative control of multiple surface vessels with discrete-time periodic communications. International Journal of Robust and Nonlinear Control. doi: 10.1002/rnc.1698,
which has been published in final form at http://onlinelibrary.wiley.com/doi/10.1002/rnc.1698/abstract.

Figure 1. The DELFIMx autonomous catamaran.

at an unprecedented scale. Besides obvious scientific applications, they can also be used in commercial operations such as automatic inspection of rubblemound breakwaters [2], bathymetry mapping for harbor safety, and remote sea floor sensing in coastal waters for marine protected area management. An example of an ASV is the DELFIMx catamaran, property of IST-ISR, that has been extensively used for marine data acquisition and in experiments with underwater acoustic systems (see Figure 1). The vessel is a major redesign of the DELFIM Catamaran, developed within the scope of the European MAST-III Asimov project that set forth the goal of achieving coordinated operation of the INFANTE AUV and the DELFIM ASV, ensuring fast data communications between the two vehicles by exploiting the vertical acoustic channel [3].

Both the DELFIM and the DELFIMx are equipped with on-board resident systems for navigation, guidance, and control, as well as mission control. Navigation is done by fusing motion data obtained with an attitude and heading reference unit and a DGPS (Differential Global Positioning System). Transmissions to and from the vehicles are achieved via serial radio links. The vehicles have a wing shaped, central structure that is lowered during operations at sea. At the bottom of this structure, a low drag body is installed that can carry acoustic transducers. For bathymetric operations and sea floor characterization, the wing may be equipped with a mechanically scanned pencil beam sonar and a sidescan sonar.

The above circle of ideas led researchers to the development of new motion control techniques designed to coordinate a group of heterogeneous vehicles (in the sense that vehicles have different dynamics and capabilities) for a wide range of practical applications [4]. Inspired by this work, the main focus of this paper is on design of a cooperative motion control system for multiple ASVs. The rest of the section sets the stage for the control design problems that we address and summarizes our main contributions.

1.2. Cooperative motion control

For our purposes, cooperative motion control is defined as the problem of making a group of vehicles follow a set of spatial paths while holding a desired geometric formation pattern. A single vehicle can follow a desired spatial path in essentially two ways. In trajectory-tracking, a vehicle is required to stay on a time-parameterized reference. In path-following, the goal is to drive a vehicle to a prescribed path without an explicit temporal constraint.

Many different approaches to the problem of cooperative motion control have been described in the literature, using a wide range of analytic tools, such as, null-space-based behavioral control [5], or Lagrange multipliers control techniques [6]. For an extended and detailed coverage of the subject, the reader is referred to [7]. Quite often, the framework adopted to tackle the problem of cooperative motion control consists of a “divide and conquer” strategy, in an attempt to decouple the problems of motion control along each spatial path and cooperation

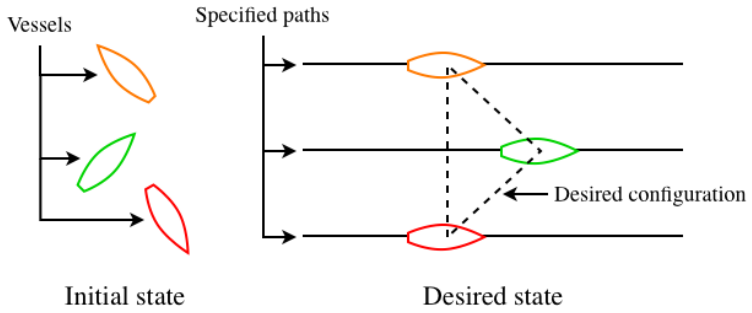

Figure 2. Illustration of the cooperative path following (CPF) concept.

along the paths. The first one is solved at a low level for each individual vehicle, while the second one is addressed at a higher level by taking into account the mission's objectives and requires communication among the vehicles. In a realistic scenario, the latter involves dealing with communication issues such as time delays, intermittent failures, transmission noise, and bandwidth restrictions.

Related work can be found in [8], where nonlinear cascaded systems theory is used to achieve straight line path-following for formations of under-actuated vehicles. In the present paper we consider fully-actuated vehicles but achieve cooperative path-following on generic smooth paths. Also relevant is the work presented in [9], where experimental results for underwater vehicles are reported. While the underwater vehicles are modeled as double integrators, the models that we adopt for surface vessels capture the dynamics of a broad class of vehicles. In the present paper we also address explicitly the constraints imposed by the inter-vehicle communications network.

1.3. Cooperative path-following

One particular type of motion control involves steering vehicles to and along desired paths without specifying a temporal law. This is known as the *path-following* control problem. As a contribution to the study of these issues, this paper addresses the *problem of cooperative path-following* (CPF) with discrete-time periodic communications, whereby a set of vehicles is required to follow pre-defined spatial paths while keeping a desired inter-vehicle formation pattern in time. To illustrate the concept of CPF, consider Figure 2. Initially, the vehicles are dispersed in space. Each vehicle is then required to converge to and follow a preassigned path and, while doing so, must position itself relative to the other vehicles in such a way that a desired spatial configuration is achieved. This problem arises, for example, in the operation of multiple autonomous underwater vehicles for fast acoustic coverage of the seabed. By imposing constraints on the inter-vehicle formation pattern, the efficacy of the task can be largely improved. At this point it is important to remark that the marine environment may pose formidable challenges to inter-vehicle communications. The problem is specially aggravated underwater, where the vehicles must communicate in short and small bursts.

Inspired by previous work on the problem of CPF (see, e.g, [10, 11, 12]), in this paper we adopt Lyapunov-based tools to address explicitly the vehicle dynamics as well as the constraints imposed by the topology of the inter-vehicle communications network. The latter are tackled in the framework of graph theory; however, unlike in [10, 11, 12], we consider communication topologies with unidirectional or directed links: one vehicle sends information to its neighbors but does not necessarily receive information back. A supporting communications network provides the vehicles with a medium to exchange information that, because of bandwidth constraints, cannot be continuous as in [10, 11], and therefore takes place only at discrete time instants that occur with a fixed frequency. We assume that the transmission delay

can be neglected and that there are no packet collisions when the vehicles communicate simultaneously.

Each vehicle is equipped with a controller that makes the vehicle follow a predefined path (see, e.g, [13, 14]). The speed of each vehicle is then adjusted so that the whole group keeps a desired formation pattern. Due to the absence of information in the intervals between transmission times, the control action of each vehicle runs in open loop, based on a simple model that predicts the evolution of its neighbors (as in Model-Based Networked Control Systems, [15]). At transmission times, each vehicle sends information through the network that is used to achieve cooperation and to update the models.

The system that is obtained by putting together the path-following and vehicle cooperation strategies takes an interconnected form, where both systems are input-to-state stable (ISS) with respect to the outputs of each other. With the control structure adopted, path-following (in space) and inter-vehicle cooperation (in time) become essentially decoupled. In fact, both control subsystems are designed separately, ignoring the signals interconnecting them, and then asymptotical stability of the closed loop system is analyzed and guaranteed using a small-gain theorem.

The paper is organized as follows. In Section 2, the dynamic model of the autonomous vehicles considered is introduced, along with key concepts from graph theory that are required to formally state the CPF problem. Section 3 is devoted to the derivation of a solution to the CPF problem. A general structure is proposed that consists of a path-following controller and a cooperation controller operating under periodic communications. In Section 4, an illustrative example is given where simulation results are presented. Finally, Section 5 contains some concluding remarks and directions for future research.

2. PROBLEM FORMULATION

The aim of this section is to formulate the problem of CPF rigorously. We will start by describing the dynamic model of the autonomous vehicles considered. Also, because more than one vehicle is involved, there is the need to take explicitly into account the topology of the underlying communication network. This can be done in the framework of graph theory, which has become the tool *par excellence* to model communication constraints in multiple vehicle mission scenarios. For this reason, we will review some key concepts and properties of graph theory (see, e.g., [16] for an in-depth presentation of this subject). After these preliminaries, we will be ready to formally state the CPF problem.

2.1. Vehicle modeling

Following standard practice, we model a surface vessel as a rigid body subjected to external forces and torques. To this effect, we let $\{\mathcal{I}\}$ be an inertial coordinate frame and $\{\mathcal{B}\}$ a body-fixed coordinate frame with its origin at the center of mass of the vehicle, as represented in Figure 3. The generalized position of the vessel is $\boldsymbol{\eta} := [x\ y\ \psi]^\top$, where x and y are the coordinates of the origin of $\{\mathcal{B}\}$ in $\{\mathcal{I}\}$ and ψ is the orientation of the vessel (yaw angle) that parameterizes the matrix

$$\mathbf{J} := \mathbf{J}(\psi) = \begin{bmatrix} \cos(\psi) & -\sin(\psi) & 0 \\ \sin(\psi) & \cos(\psi) & 0 \\ 0 & 0 & 1 \end{bmatrix},$$

transforming body coordinates into inertial coordinates. Denote by $\boldsymbol{\nu} := [u\ v\ r]^\top$ the generalized velocity of the vessel relative to $\{\mathcal{I}\}$ expressed in $\{\mathcal{B}\}$. The following *kinematic* relations apply:

$$\dot{\boldsymbol{\eta}} = \mathbf{J}\boldsymbol{\nu}, \tag{1}$$

$$\dot{\mathbf{J}} = r\mathbf{J}\mathbf{S}, \tag{2}$$

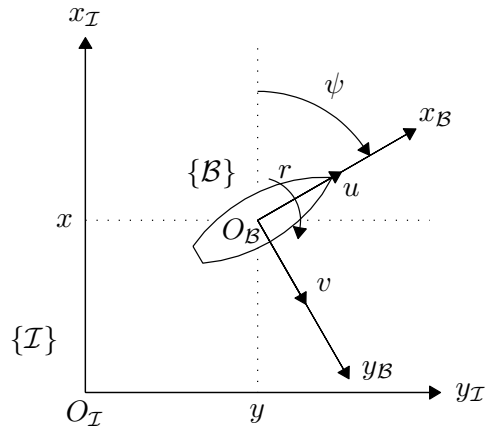

Figure 3. Inertial and body-fixed coordinate frames.

where $\mathbf{S}$ is the skew-symmetric matrix

$$\mathbf{S} = \begin{bmatrix} 0 & -1 & 0 \\ 1 & 0 & 0 \\ 0 & 0 & 0 \end{bmatrix}; (\mathbf{S}^\top = -\mathbf{S}).$$

We consider a fully-actuated vessel with simplified *dynamic* equations of motion of the form [17]

$$\mathbf{M}\dot{\boldsymbol{\nu}} = \boldsymbol{\tau} + \boldsymbol{f}(\boldsymbol{\eta}, \boldsymbol{\nu}), \tag{3}$$

where $\mathbf{M} \in \mathbb{R}^{3\times 3}$ denotes a constant symmetric positive definite mass matrix, $\boldsymbol{\tau} := [\tau_u \ \tau_v \ \tau_r]^\top$ is the generalized control input consisting of forces τ_u, τ_v, and torque τ_r, and $\boldsymbol{f}(\boldsymbol{\eta}, \boldsymbol{\nu})$ represents Coriolis, centripetal, and hydrodynamic damping forces and torques acting on the body. For the special case of surface vessels, $\mathbf{M}$ also includes the so-called hydrodynamic added-mass $\mathbf{M}_A$, i.e., $\mathbf{M} = \mathbf{M}_{RB} + \mathbf{M}_A$, where $\mathbf{M}_{RB}$ is the rigid-body mass matrix.

2.2. Graph theory

This section contains some key concepts and results in graph theory that play an important role in what follows. A directed graph or digraph $\mathcal{G} = \mathcal{G}(\mathcal{V}, \mathcal{E})$ consists of a finite set $\mathcal{V} = \{1, 2, \ldots, n\}$ of n vertices and a finite set $\mathcal{E}$ of m ordered pairs of vertices $(i, j) \in \mathcal{E}$ named arcs. Given an arc $(i, j) \in \mathcal{E}$, its first and second elements are called the tail and head of the arc, respectively. The out-degree of a vertex i is the number of arcs with i as its tail. If (i, j) belongs to $\mathcal{E}$ then we say that i is adjacent to j. A path from i to j is a sequence of distinct vertices starting with i and ending with j such that consecutive vertices are adjacent. If there is a path in $\mathcal{G}$ from vertex i to vertex j, then j is said to be reachable from i. A vertex i is globally reachable if it is reachable from every other vertex in $\mathcal{G}$. The adjacency matrix of a digraph, denoted $\mathbf{A}$, is a square matrix with rows and columns indexed by the vertices, such that the i, j-entry of $\mathbf{A}$ is 1 if $(i, j) \in \mathcal{E}$ and 0 otherwise. The out-degree matrix $\mathbf{D}$ of a digraph is a diagonal matrix where the i, i-entry is equal to the out-degree of vertex i, that is, $\mathbf{D} = \mathrm{diag}(\mathbf{A}\mathbf{1})$ where $\mathbf{1} = [1]_{n\times 1}$ is a vector of ones.

The Laplacian of a digraph is defined as $\mathbf{L} = \mathbf{D} - \mathbf{A}$. By definition, the Laplacian satisfies $\mathbf{L}\mathbf{1} = \mathbf{0}$, and therefore 0 is an eigenvalue of $\mathbf{L}$ with $\mathbf{1}$ being its associated right eigenvector. In [18], it is shown that a digraph has at least one globally reachable vertex if and only if zero is a simple eigenvalue of $\mathbf{L}$ (all other eigenvalues have positive real parts). This implies that $\mathrm{rank}\,\mathbf{L} = n - 1$ for a graph with at least one globally reachable vertex. Hence, there exist matrices $\mathbf{F} \in \mathbb{R}^{n\times(n-1)}$ and $\mathbf{G} \in \mathbb{R}^{(n-1)\times n}$ such that $\mathbf{L} = \mathbf{F}\mathbf{G}$, where $\mathrm{rank}\,\mathbf{F} = \mathrm{rank}\,\mathbf{G} = n - 1$, and $\mathbf{G}\mathbf{1} = \mathbf{0}$.

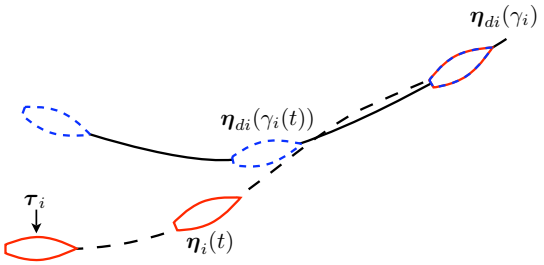

Figure 4. Illustration of path-following from the point-of-view of vessel i. By changing the control input $\boldsymbol{\tau}_i$, the vessel should converge to a "virtual" vessel that moves along the preassigned path.

2.3. Problem statement

Consider a set of $n \geq 2$ autonomous surface vessels and a set of n spatial paths

$$\{\boldsymbol{\eta}_{di}(\gamma_i) := [x_{di}(\gamma_i)\ y_{di}(\gamma_i)\ \psi_{di}(\gamma_i)]^\top \in \mathbb{R}^3 : i = 1, 2, \ldots, n\},$$

where each path $\boldsymbol{\eta}_{di}$ is parameterized by a continuous variable $\gamma_i \in \mathbb{R}$ and consists of a desired position specified by x_{di} and y_{di} and a desired yaw angle ψ_{di}. It is common to take γ_i as the arc length of the ith path. However, it may be necessary to reparameterize the path, as explained below. The path-following part of the CPF problem consists of driving each ith vessel to its assigned path $\boldsymbol{\eta}_{di}$. See Figure 4 for a graphical illustration.

To formalize the notion of cooperation, we start by introducing a measure of the degree of cooperation of a fleet of vehicles. As in [11], this is done by reparameterizing each path $\boldsymbol{\eta}_{di}(\gamma_i)$ in terms of a conveniently defined variable ξ_i such that cooperation is said to be achieved along the paths if and only if $\xi_1 = \xi_2 = \ldots = \xi_n$. At this point, we formally define the "along-path" distances between vehicle i and j as $\xi_{i,j} = \xi_i - \xi_j$. Then, cooperation is achieved if and only if $\xi_{i,j} = 0$ for all $i, j \in \{1, 2, \ldots, n\}$. Formally, let the reparameterization of the path be represented by $\gamma_i = \gamma_i(\xi_i)$ and define $R_i(\xi_i) := \partial\gamma_i/\partial\xi_i$, which is assumed to be positive and bounded for all ξ_i. Clearly, the dynamics of ξ_i and γ_i are related by

$$\dot{\gamma}_i = R_i(\xi_i)\dot{\xi}_i\,. \tag{4}$$

This paper considers the case where $R_i(\xi_i)$ is constant. While restrictive, it still allows us to consider paths where there is no need for reparameterization (that is, $\xi_i = \gamma_i$) or the parameterization amounts to a constant scaling. The latter happens, for example, when considering cooperation along concentric circumferences as depicted in Figure 5. If γ_i represents the arc length of the corresponding circumference, then ξ_i is obtained by dividing γ_i by the corresponding circumference's radius. Thus, ξ_i is equal to the angular position of vessel i along the circumference.

Suppose one vessel, henceforth referred to as vessel $\mathcal{L}$, is elected as the "leader" and let the corresponding path $\eta_{d\mathcal{L}}$ be parameterized by $\gamma_\mathcal{L} = \xi_\mathcal{L}$. For this vessel, $R_\mathcal{L} = 1$. Let $v_\mathcal{L}$ be the desired constant speed assigned to the leader in advance, that is $\dot{\xi}_\mathcal{L} = v_\mathcal{L}$ in steady-state, known to all vessels. From (4), it follows that the desired "along-path" speeds for the vessels are $v_{di} := R_i v_\mathcal{L}$. It is important to point out that $\mathcal{L}$ can always be taken as a "virtual" vehicle that is added to the set of "real" vehicles as an expedient to simplify the cooperation strategy.

So far, the problem of cooperation has been reduced to that of aligning, in an appropriate sense, the cooperation states ξ_i. To go from this in-line configuration to a more complex one, we introduce appropriate offsets in the desired positions of the vessels relative to the mean point of the formation as defined with respect to the paths. To this effect, let $\boldsymbol{\xi} := [\xi_i]_{n\times 1}$ and define the formation mean point and offsets as $\bar{\xi} := \frac{1}{n}\mathbf{1}^\top\boldsymbol{\xi}$ and $\boldsymbol{\delta} := \boldsymbol{\xi} - \bar{\xi}\mathbf{1}$, respectively. Notice that $\mathbf{1}^\top\boldsymbol{\delta} = 0$. Let $\boldsymbol{\phi} \in \mathbb{R}^n$ represent a desired constant formation pattern that verifies $\mathbf{1}^\top\boldsymbol{\phi} = 0$. The problem of cooperation with pattern tracking is reduced to that of making $(\boldsymbol{\delta} - \boldsymbol{\phi}) \to \mathbf{0}$ as $t \to +\infty$. See Figure 6 for a possible spatial configuration.

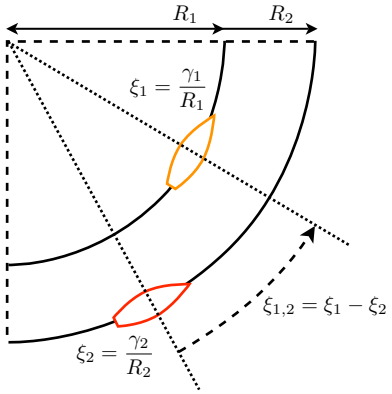

Figure 5. Cooperation along concentric circumferences. The γ_i variables represent the arc length of the corresponding circumference while the ξ_i variables are the angular position relative to the circumferences' center.

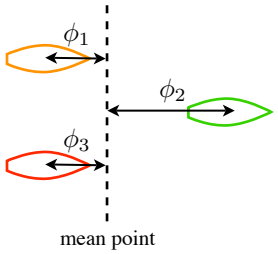

Figure 6. Example of spatial configuration: wedge formation, $\boldsymbol{\phi} = (-1, 2, -1)$.

From a graph theoretical point of view, each vessel is represented by a vertex and a communication link between two vessels is represented by an arc. The communication links are assumed unidirectional, thereby inducing a directed graph. We consider time-invariant communication topologies and assume that the induced graph has at least one globally reachable vertex. The flow of information in an arc is directed from its head to its tail. The set of neighbors of vertex i is represented by $\mathcal{N}_i$ and contains all vertices j such that $(i, j) \in \mathcal{E}$. In other words, it is the group of vessels from which vessel i receives information.

For design purposes, we will take each $\dot{\xi}_i$ as a control input in the cooperation dynamics (4). In order to satisfy the constraints imposed by the topology of the communication network, the control law for vessel i must be *decentralized*, i.e, it may only depend on local states and/or on information exchange with its neighbors as specified by $\mathcal{N}_i$.

To summarize, the cooperative path-following problem is formally stated next.

Problem (Cooperative Path-Following)
Consider a set of n vessels with equations of motion defined by (1)-(3). Let $\boldsymbol{\eta}_{di}(\gamma_i) \in \mathbb{R}^3$ be desired paths parameterized by continuous variables $\gamma_i \in \mathbb{R}$ and let $v_{\mathcal{L}} \in \mathbb{R}$ be a desired reference speed assignment. Assume each $\boldsymbol{\eta}_{di}(\gamma_i)$ is sufficiently smooth and its derivatives with respect to γ_i are bounded. Let the desired multiple vehicle formation pattern be defined by $\boldsymbol{\phi} \in \mathbb{R}^n$. Then, design control laws for $\boldsymbol{\tau}_i$ and a decentralized feedback law for $\dot{\boldsymbol{\xi}}$ such that:

1. all closed-loop signals are bounded (*stability*);
2. the position of each vessel converges to the corresponding desired path, that is, $\|\boldsymbol{\eta}_i(t) - \boldsymbol{\eta}_{di}(\gamma_i(t))\| \to 0$ as $t \to +\infty$ (*path-following*); and,
3. the desired formation pattern is acquired and all vessels travel at the desired along-path speed, that is, $\boldsymbol{\delta} - \boldsymbol{\phi} \to 0$ and $\dot{\gamma}_i \to v_{di}$ for all $i \in \{1, 2, \ldots, n\}$ as $t \to +\infty$ (*cooperation*).

Notice that the cooperation part of the CPF problem that we posed is closely related to agreement problems (see, e.g., [19]). In our case, all vehicles must agree on a common value that is the mean point of the formation pattern.

3. CONTROLLER DESIGN

In this section, we start by presenting the general structure of the proposed CPF controller. It consists of a path-following controller and a cooperation controller operating under periodic communications. Both control subsystems are designed separately, ignoring the signals interconnecting them; asymptotic stability of the closed loop system is proven exploiting concepts from input-to-state stability and a small-gain theorem (see, e.g, [20, 21]) concepts that are briefly reviewed in the following subsection.

3.1. Small-gain theorem

Let $\boldsymbol{x}$ denote the state of a system described by

$$\dot{\boldsymbol{x}} = \boldsymbol{f}(\boldsymbol{x}, \boldsymbol{u}). \tag{5}$$

We will use the following simplified notion of input-to-state stability. System (5) is said to be *input-to-state stable* (ISS), with respect to state $\boldsymbol{x}$ and input $\boldsymbol{u}$, if there exist positive constants κ, λ, and σ such that, for any initial condition $\boldsymbol{x}(t_0)$ and any bounded input $\boldsymbol{u}$, the solution $\boldsymbol{x}(t)$ exists and satisfies

$$\|\boldsymbol{x}(t)\| \leq \kappa e^{-\lambda(t-t_0)}\|\boldsymbol{x}(t_0)\| + \sigma\|\boldsymbol{u}\|_{[t_0,t]}$$

for all $t \geq t_0$, where

$$\|\boldsymbol{u}\|_{[t_0,t]} := \sup_{s\in[t_0,t]} \|\boldsymbol{u}(s)\|.$$

Now, consider the interconnected system

$$\dot{\boldsymbol{x}}_1 = \boldsymbol{f}_1(\boldsymbol{x}_1, \boldsymbol{x}_2), \tag{6}$$
$$\dot{\boldsymbol{x}}_2 = \boldsymbol{f}_2(\boldsymbol{x}_1, \boldsymbol{x}_2). \tag{7}$$

Suppose subsystem (6) is ISS with respect to state $\boldsymbol{x}_1$ and input $\boldsymbol{x}_2$, with constants κ_1, λ_1, and σ_1. Further assume that subsystem (7) is also ISS with respect to state $\boldsymbol{x}_2$ and input $\boldsymbol{x}_1$, with constants κ_2, λ_2, and σ_2. The following is a simplified presentation of the ISS small-gain theorem in [20, 21].

Theorem 1 (Small-gain)
If the positive constants σ_1 and σ_2 satisfy

$$\sigma_1\sigma_2 < 1$$

then the interconnected system (6)-(7), with state $\boldsymbol{x} = [\boldsymbol{x}_1^\top \ \boldsymbol{x}_2^\top]^\top$, is globally asymptotically stable.

3.2. Control structure

In this section we propose a control structure for the CPF problem that builds on the work in [10] and is illustrated in Figure 7 for the ith vessel. The structure proposed is the interconnection of two subsystems: the path-following (PF) subsystem and the cooperation control (CC) subsystem.

The PF subsystem is formed by the vessel itself and a state feedback controller designed to guide it to the desired path. The PF controller drives the vehicle through its command input $\boldsymbol{\tau}_i$ using a control law that depends on the vehicle's position $\boldsymbol{\eta}_i$ and velocity $\boldsymbol{\nu}_i$, and on signals

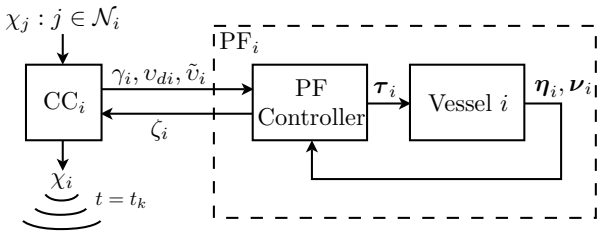

Figure 7. Proposed control structure for CPF from the point-of-view of vessel i.

provided by the CC subsystem. It also provides the CC subsystem with a feedback signal ζ_i to be defined later.

The CC subsystem handles all the communications with neighboring vessels and provides the PF subsystem with the parameterizing variable γ_i, the desired along-path speed υ_{di}, and the signal $\tilde{\upsilon}_i$ to be defined in the sequel. The exchange of information occurs at discrete-time instants $\{t_k = hk + t_0 : k \in \mathbb{N}\}$, that will henceforth be referred to as *update times*, where h is the communication period in seconds. At these update times, a certain information variable χ_i, to be defined later, is sent by vessel i to its adjacent vehicles and information variables $\chi_j : j \in \mathcal{N}_i$ from its neighbors are received. These information variables constitute the only data that must be exchanged among vessels to achieve cooperation. We consider dynamic equations for γ_i of the form

$$\dot{\gamma}_i = \upsilon_{di} + \tilde{\upsilon}_i + \zeta_i \tag{8}$$

where $\upsilon_{di} := R_i \upsilon_{\mathcal{L}}$ is the desired speed for vessel i, $\tilde{\upsilon}_i$ is a control signal to be chosen in order to solve the cooperation problem (as a function of χ_i and $\chi_j : j \in \mathcal{N}_i$), and ζ_i is a signal from the PF subsystem that will be treated as an external input.

The PF subsystem will be shown to be ISS with respect to state $\boldsymbol{x}_{Pi}$ (which represents the state of the PF subsystem of vessel i) and input $\tilde{\upsilon}_i$. The CC subsystem will be shown to be ISS with respect to state $\boldsymbol{x}_{Ci}$ (which represents the state of the CC subsystem of vessel i) and input ζ_i.

A sampled-data based approach to the problem of cooperative path-following was proposed in [12], where the variables parameterizing the paths (γ_i) evolve in a discrete fashion, and therefore the cooperation control problem is posed in discrete-time. However, the authors only considered communication topologies with bidirectional links.

3.3. Path-following

Central to the development of CPF strategies is the derivation of appropriate path-following control laws for each vehicle. In this section we present a path-following controller for an autonomous surface vessel described by the equations of motions introduced in Section 2.1, the structure of which bears affinity with those proposed in [13, 14]. The controller is local to each vehicle and therefore the index i will be omitted for the sake of clarity.

Let the position error in the body-fixed frame be denoted as $\boldsymbol{z}_1 := \mathbf{J}^\top(\boldsymbol{\eta} - \boldsymbol{\eta}_d)$. The goal of the path-following controller is to drive $\boldsymbol{z}_1$ to zero. Applying backstepping design procedures (see, e.g, [22]), the Lyapunov function

$$V := \frac{1}{2}\boldsymbol{z}_1^\top \boldsymbol{z}_1 + \frac{1}{2}\boldsymbol{z}_2^\top \mathbf{M} \boldsymbol{z}_2, \tag{9}$$

yields the feedback control law

$$\boldsymbol{\tau} = -\boldsymbol{z}_1 - \mathbf{K}_2 \boldsymbol{z}_2 - \boldsymbol{f} + \mathbf{M}(\boldsymbol{\alpha}^t + \boldsymbol{\alpha}^\gamma \dot{\gamma}), \tag{10}$$

$$\zeta = -w\mu, \tag{11}$$

where

$$\begin{aligned}
\boldsymbol{z}_2 &:= \boldsymbol{\nu} - \boldsymbol{\alpha},\\
\mu &:= -(\boldsymbol{\eta}_d^{\gamma})^{\top}\mathbf{J}\boldsymbol{z}_1,\\
\boldsymbol{\alpha} &:= \mathbf{J}^{\top}\boldsymbol{\eta}_d^{\gamma}\upsilon_d - \mathbf{K}_1\boldsymbol{z}_1,\\
\boldsymbol{\alpha}^{\gamma} &:= \mathbf{K}_1\mathbf{J}^{\top}\boldsymbol{\eta}_d^{\gamma} + \mathbf{J}^{\top}\boldsymbol{\eta}_d^{\gamma^2}\upsilon_d,\\
\boldsymbol{\alpha}^{t} &:= -\mathbf{K}_1(\boldsymbol{\nu} - r\mathbf{S}\boldsymbol{z}_1) - r\mathbf{S}\mathbf{J}^{\top}\boldsymbol{\eta}_d^{\gamma}\upsilon_d + \mathbf{J}^{\top}\boldsymbol{\eta}_d^{\gamma}\dot{\upsilon}_d,
\end{aligned}$$

$\boldsymbol{\eta}_d^{\gamma^p} = \partial^p\boldsymbol{\eta}_d/\partial\gamma^p$ with $p = 1, 2$, and $\mathbf{K}_1, \mathbf{K}_2, w$ are controller gains. Using (10) and (11) as feedback laws, the time derivative of (9) along the solutions of (1)-(3) becomes

$$\dot{V} = -\boldsymbol{z}_1^{\top}\mathbf{K}_1\boldsymbol{z}_1 - \boldsymbol{z}_2^{\top}\mathbf{K}_2\boldsymbol{z}_2 - w\mu^2 + \mu\tilde{\upsilon}. \tag{12}$$

The closed loop system with $\tilde{\upsilon}$ as input has an important property stated in the next lemma.

Lemma 1
The PF subsystem described is ISS with respect to state $\boldsymbol{x}_P = [\boldsymbol{z}_1^{\top}\ \boldsymbol{z}_2^{\top}]^{\top} \in \mathbb{R}^6$ and input $\tilde{\upsilon}$, that is,

$$\|\boldsymbol{x}_P(t)\| \leq \kappa_P e^{-\lambda_P(t-t_0)}\|\boldsymbol{x}_P(t_0)\| + \sigma_P|\tilde{\upsilon}|_{[t_0,t]}$$

for some positive constants κ_P, λ_P, and σ_P. Moreover, σ_P can be made arbitrary small by increasing the PF gains $\mathbf{K}_1$ and $\mathbf{K}_2$.

Proof
Let $k_i = \lambda_{\min}(\mathbf{K}_i)$ for $i = 1, 2$. Using the fact that the desired path is bounded, $|\mu| \leq \beta_1\|\boldsymbol{z}_1\|$ for some positive constant β_1. Hence (12) can be upper bounded by

$$\begin{aligned}
\dot{V} &\leq -k_1\|\boldsymbol{z}_1\|^2 - k_2\|\boldsymbol{z}_2\|^2 - w\mu^2 + |\mu||\tilde{\upsilon}|\\
&\leq -(k_1 + w\beta_1^2)\|\boldsymbol{z}_1\|^2 - k_2\|\boldsymbol{z}_2\|^2 + \beta_1\|\boldsymbol{z}_1\||\tilde{\upsilon}|.
\end{aligned}$$

Let $\tilde{k}_1 = k_1 + w\beta_1^2$. Applying Young's inequality* to the term $\|\boldsymbol{z}_1\||\tilde{\upsilon}|$, we get

$$\begin{aligned}
\dot{V} &\leq -\tilde{k}_1\|\boldsymbol{z}_1\|^2 - k_2\|\boldsymbol{z}_2\|^2 + \beta_1\Big(\frac{1}{4\delta}\|\boldsymbol{z}_1\|^2 + \delta|\tilde{\upsilon}|^2\Big)\\
&= -\Big(\tilde{k}_1 - \frac{\beta_1}{4\delta}\Big)\|\boldsymbol{z}_1\|^2 - k_2\|\boldsymbol{z}_2\|^2 + \beta_1\delta|\tilde{\upsilon}|^2.
\end{aligned}$$

Let $\delta = \frac{\beta_1}{2\tilde{k}_1}$ and $\sigma = \beta_1\delta$. Then,

$$\begin{aligned}
\dot{V} &\leq -\frac{1}{2}\tilde{k}_1\|\boldsymbol{z}_1\|^2 - k_2\|\boldsymbol{z}_2\|^2 + \sigma|\tilde{\upsilon}|^2\\
&\leq -\alpha\|\boldsymbol{x}_P\|^2 + \sigma|\tilde{\upsilon}|^2
\end{aligned}$$

where $\alpha = \min\{\frac{1}{2}\tilde{k}_1, k_2\}$. Using the fact that

$$\alpha_1\|\boldsymbol{x}_P\|^2 \leq V(\boldsymbol{x}_P) \leq \alpha_2\|\boldsymbol{x}_P\|^2$$

with $\alpha_1 = \frac{1}{2}\min\{1, \lambda_{\min}(\mathbf{M})\}$ and $\alpha_2 = \frac{1}{2}\max\{1, \lambda_{\max}(\mathbf{M})\}$, straightforward computations allow for the conclusion that

$$\|\boldsymbol{x}_P(t)\| \leq \kappa_P e^{-\lambda_P(t-t_0)}\|\boldsymbol{x}_P(t_0)\| + \sigma_P|\tilde{\upsilon}|_{[t_0,t]},$$

with

$$\kappa_P = \sqrt{\frac{\alpha_2}{\alpha_1}},\ \lambda_P = \frac{\alpha}{2\alpha_2},\ \text{and}\ \sigma_P = \sqrt{\frac{\alpha_2\sigma}{\alpha_1\alpha}}.$$

Therefore, the PF subsystem is ISS with respect to state $\boldsymbol{x}_P$ and input $\tilde{\upsilon}$. Note that if k_1 and k_2 are both increased, then α will increase and σ will decrease, thus decreasing σ_P. □

*One of several possible formulations states that given $a, b \in \mathbb{R}$ and $\delta > 0$ then $ab \leq \frac{1}{4\delta}a^2 + \delta b^2$.

3.4. Cooperation control

We now focus our attention on the cooperative aspect of the CPF problem. Rewriting (8) in terms of $\dot{\xi}_i$ and using a control law for $\tilde{v}_i$ adapted from [11], we obtain the following controller that solves the cooperation problem under continuous communications:

$$\dot{\xi}_i = v_{\mathcal{L}} + R_i^{-1}(\tilde{v}_i + \zeta_i), \tag{13}$$

$$\tilde{v}_i = -k_{ci} \sum_{j \in \mathcal{N}_i} (\xi_i - \phi_i - \xi_j + \phi_j), \tag{14}$$

where $k_{ci} > 0$ is an adjustable control gain and ϕ_i are the components of the desired formation pattern represented by $\boldsymbol{\phi}$. Notice that the information required by vessel i about its neighbors is $\chi_j := \xi_j - \phi_j$, that we refer to as *information state*, and not the cooperation state ξ_j itself. The control law (13) can be rewritten as

$$\dot{\chi}_i = v_{\mathcal{L}} + R_i^{-1}(\tilde{v}_i + \zeta_i), \tag{15}$$

$$\tilde{v}_i = -k_{ci} d_i \chi_i + k_{ci} \sum_{j \in \mathcal{N}_i} \chi_j, \tag{16}$$

where d_i is the number of neighbors of vessel i (out-degree of vertex i) and $k_{ci} = 0$ if $d_i = 0$. When using periodic communications, the vessel i does not receive $\{\chi_j : j \in \mathcal{N}_i\}$ between update times, so it needs to model their evolution in that interval. Let $\hat{\chi}_j^i$ represent a local "replica" of each χ_j as seen by vessel i, that we refer to as *predictor state*. Analyzing (15), we see that if a steady-state condition is achieved, then $\dot{\chi}_i = v_{\mathcal{L}}$ for all i. This suggests that the dynamics of χ_j can be predicted as $\dot{\hat{\chi}}_j^i = v_{\mathcal{L}}$, thus yielding the controller

$$\tilde{v}_i = -k_{ci} d_i \chi_i + k_{ci} \sum_{j \in \mathcal{N}_i} \hat{\chi}_j^i, \tag{17}$$

$$\dot{\hat{\chi}}_j^i = v_{\mathcal{L}}, \text{ for each } j \in \mathcal{N}_i\,. \tag{18}$$

However, this is not sufficient to achieve cooperation due to initial conditions that do not match the desired formation pattern. To overcome this problem, a reset is made to the predictor states when information is exchanged. We therefore add the following condition to the controller:

$$\hat{\chi}_j^i(t_k) = \chi_j^i(t_k^-), \text{ for all } j \in \mathcal{N}_i, \tag{19}$$

where the notation $x(t^-)$ stands for the left limit or limit from below, i.e., $x(t^-) = \lim_{s \nearrow t} x(s)$. Because all $\hat{\chi}_j^i$ are initialized with the same value $\chi_j(t_0)$, and because we assume there is absolute synchronization with respect to update times, vehicles that model the same predictor state have equal values, i.e, $\hat{\chi}_j^{i_1} = \hat{\chi}_j^{i_2}$ for all i_1, i_2, and j. Therefore, we do not need to refer to $\hat{\chi}_j^{i_1}$ and $\hat{\chi}_j^{i_2}$ as different states, we simply refer to them as $\hat{\chi}_j$.

Defining $\hat{\boldsymbol{\chi}} := \boldsymbol{\xi} - \boldsymbol{\phi} = [\hat{\chi}_i]_{n\times 1}$, $\boldsymbol{\zeta} := [\zeta_i]_{n\times 1}$, the diagonal matrices $\mathbf{K}_c := \mathrm{diag}[k_{ci}]_{n\times n}$, and $\mathbf{C} := \mathrm{diag}[R_i^{-1}]_{n\times n}$, equations (17)-(19) can be written in vector form as

$$\dot{\boldsymbol{\chi}} = v_{\mathcal{L}}\mathbf{1} + \mathbf{C}(-\mathbf{K}_c\mathbf{D}\boldsymbol{\chi} + \mathbf{K}_c\mathbf{A}\hat{\boldsymbol{\chi}} + \boldsymbol{\zeta}), \tag{20}$$

$$\dot{\hat{\boldsymbol{\chi}}} = v_{\mathcal{L}}\mathbf{1}, \tag{21}$$

$$\hat{\boldsymbol{\chi}}(t_k) = \boldsymbol{\chi}(t_k^-)\,. \tag{22}$$

The cooperation error is defined as

$$\boldsymbol{\theta} := \mathbf{G}(\boldsymbol{\xi} - \boldsymbol{\phi}) = \mathbf{G}\boldsymbol{\chi} \in \mathbb{R}^{n-1},$$

where $\mathbf{G}$ is obtained from the decomposition of the Laplacian discussed in Section 2.2. Since $\mathbf{G}\mathbf{1} = \mathbf{0}$, using the definitions of formation mean point and offsets of Section 2.3 yields

$$\mathbf{G}(\boldsymbol{\xi} - \boldsymbol{\phi}) = \mathbf{G}(\boldsymbol{\delta} + \bar{\xi}\mathbf{1} - \boldsymbol{\phi}) = \mathbf{G}(\boldsymbol{\delta} - \boldsymbol{\phi})\,.$$

Because $\mathbf{1}^\top \boldsymbol{\delta} = \mathbf{1}^\top \boldsymbol{\phi} = 0$, $\boldsymbol{\delta} - \boldsymbol{\phi}$ is normal to the null space of $\mathbf{G}$. We conclude that $\boldsymbol{\theta} = \mathbf{0}$ if and only if $(\boldsymbol{\delta} - \boldsymbol{\phi}) = \mathbf{0}$. Let

$$\tilde{\boldsymbol{\chi}} := \boldsymbol{\chi} - \hat{\boldsymbol{\chi}} \in \mathbb{R}^n$$

represent the predictor state error. If $\tilde{\boldsymbol{\chi}} = \mathbf{0}$, then the information states are coherent, i.e, the predictor states equal the actual states. Considering (20)-(22), the error dynamics for $\boldsymbol{\theta}$ and $\tilde{\boldsymbol{\chi}}$ are given by

$$\begin{aligned}
\dot{\tilde{\boldsymbol{\chi}}} &= -\mathbf{C}\mathbf{K}_c\mathbf{F}\boldsymbol{\theta} - \mathbf{C}\mathbf{K}_c\mathbf{A}\tilde{\boldsymbol{\chi}} + \mathbf{C}\boldsymbol{\zeta}, \\
\dot{\boldsymbol{\theta}} &= -\mathbf{G}\mathbf{C}\mathbf{K}_c\mathbf{F}\boldsymbol{\theta} - \mathbf{G}\mathbf{C}\mathbf{K}_c\mathbf{A}\tilde{\boldsymbol{\chi}} + \mathbf{G}\mathbf{C}\boldsymbol{\zeta},
\end{aligned}$$

where we used the fact that $\mathbf{L}\boldsymbol{\chi} = \mathbf{F}\mathbf{G}\boldsymbol{\chi} = \mathbf{F}\boldsymbol{\theta}$. Defining the aggregated state variable $\boldsymbol{x}_C := [\boldsymbol{\theta}^\top \ \tilde{\boldsymbol{\chi}}^\top]^\top$, the above error dynamics can be written as

$$\begin{cases}
\dot{\boldsymbol{x}}_C = \boldsymbol{\Lambda}\boldsymbol{x}_C + \mathbf{B}\boldsymbol{\zeta}, & t \in [t_k, t_{k+1}) \quad (23) \\
\boldsymbol{x}_C(t) = (\boldsymbol{\theta}(t^-), \mathbf{0}), & t = t_k \quad (24)
\end{cases}$$

where

$$\boldsymbol{\Lambda} := \begin{bmatrix} -\mathbf{G}\mathbf{C}\mathbf{K}_c\mathbf{F} & -\mathbf{G}\mathbf{C}\mathbf{K}_c\mathbf{A} \\ -\mathbf{C}\mathbf{K}_c\mathbf{F} & -\mathbf{C}\mathbf{K}_c\mathbf{A} \end{bmatrix}, \tag{25}$$

$$\mathbf{B} := \begin{bmatrix} \mathbf{G}\mathbf{C} \\ \mathbf{C} \end{bmatrix}. \tag{26}$$

The dynamic system (23)-(24) is a linear impulsive system.

We now introduce some definitions and notation. We denote an *open disk* in the complex plane as $\mathcal{D}(c, r) := \{x \in \mathbb{C} : |x - c| < r\}$ with center $c \in \mathbb{C}$ and radius $r > 0$. Similarly, a *closed disk* is denoted as $\overline{\mathcal{D}}(c, r) := \{x \in \mathbb{C} : |x - c| \leq r\}$. The set of distinct eigenvalues or *spectrum* of a matrix $\mathbf{X}$ is represented by $\sigma(\mathbf{X})$. A matrix $\mathbf{X}$ is called a *convergent matrix* if all its eigenvalues are strictly inside the unit circle, i.e., if $\sigma(\mathbf{X}) \subseteq \mathcal{D}(0, 1)$.

Theorem 2
The system described by (23)-(24) is ISS with respect to state $\boldsymbol{x}_C$ and input $\boldsymbol{\zeta}$ if

$$\boldsymbol{\Phi} := \begin{bmatrix} \mathbf{I}_{n-1} & 0 \\ 0 & 0 \end{bmatrix} e^{\boldsymbol{\Lambda} h} \tag{27}$$

is a convergent matrix.

Before proving the theorem, some lemmas must be introduced. The following lemma shows that $\boldsymbol{\Lambda}$ is similar to a diagonal matrix.

Lemma 2
Consider the matrix $\boldsymbol{\Lambda}$ defined in (25). Let $\mathbf{P}, \boldsymbol{\Delta} \in \mathbb{R}^{(2n-1)\times(2n-1)}$ be defined as

$$\boldsymbol{\Delta} := \begin{bmatrix} -\mathbf{C}\mathbf{K}_c\mathbf{D} & \mathbf{0}_{n\times(n-1)} \\ \mathbf{0}_{(n-1)\times n} & \mathbf{0}_{n-1} \end{bmatrix}, \ \mathbf{P} := \begin{bmatrix} \mathbf{G} & \mathbf{I}_{n-1} - \mathbf{G}\mathbf{D}^+\mathbf{F} \\ \mathbf{I}_n & -\mathbf{D}^+\mathbf{F} \end{bmatrix},$$

where $\mathbf{D}^+ = \operatorname{diag}(d_1^+, \ldots, d_n^+)$ stands for the pseudoinverse of $\mathbf{D}$, with

$$d_i^+ := \begin{cases} d_i^{-1}, & \text{if } d_i > 0 \\ 0, & \text{if } d_i = 0 \end{cases}$$

for $i = 1, 2, \ldots, n$. Then, $\mathbf{P}$ is nonsingular with inverse given by

$$\mathbf{P}^{-1} = \begin{bmatrix} \mathbf{D}^+\mathbf{F} & \mathbf{I}_{n-1} - \mathbf{D}^+(\mathbf{D} - \mathbf{A}) \\ \mathbf{I}_{n-1} & -\mathbf{G} \end{bmatrix}$$

and $\boldsymbol{\Lambda} = \mathbf{P}\boldsymbol{\Delta}\mathbf{P}^{-1}$.

Proof
From $\mathbf{P}\mathbf{P}^{-1} = \mathbf{P}^{-1}\mathbf{P} = \mathbf{I}_{2n-1}$ it follows that $\mathbf{P}$ is nonsingular with inverse $\mathbf{P}^{-1}$. Straightforward computations yield

$$\mathbf{P}\boldsymbol{\Delta}\mathbf{P}^{-1} = \begin{bmatrix} -\mathbf{G}\mathbf{C}\mathbf{K}_c\mathbf{D}\mathbf{D}^{+}\mathbf{F} & -\mathbf{G}\mathbf{C}\mathbf{K}_c\mathbf{D}(\mathbf{I}_n - \mathbf{D}^{+}(\mathbf{D}-\mathbf{A})) \\ -\mathbf{C}\mathbf{K}_c\mathbf{D}\mathbf{D}^{+}\mathbf{F} & -\mathbf{C}\mathbf{K}_c\mathbf{D}(\mathbf{I}_n - \mathbf{D}^{+}(\mathbf{D}-\mathbf{A})) \end{bmatrix}.$$

It is easy to show that

$$\begin{aligned} \mathbf{C}\mathbf{K}_c\mathbf{D}(\mathbf{I}_n - \mathbf{D}^{+}(\mathbf{D}-\mathbf{A})) &= \mathbf{C}\mathbf{K}_c\mathbf{D} - \mathbf{C}\mathbf{K}_c\mathbf{D}\mathbf{D}^{+}(\mathbf{D}-\mathbf{A}) \\ &= \mathbf{C}\mathbf{K}_c\mathbf{D} - \mathbf{C}\mathbf{K}_c\mathbf{D}\mathbf{D}^{+}\mathbf{D} + \mathbf{C}\mathbf{K}_c\mathbf{A} \\ &= \mathbf{C}\mathbf{K}_c\mathbf{A}, \end{aligned}$$

where we used the facts that $\mathbf{D}\mathbf{D}^{+}\mathbf{D} = \mathbf{D}$, $\mathbf{D}\mathbf{D}^{+}\mathbf{A} = \mathbf{A}$ and $\mathbf{C}\mathbf{K}_c\mathbf{D}\mathbf{D}^{+} = \mathbf{C}\mathbf{K}_c$. Therefore,

$$\mathbf{P}\boldsymbol{\Delta}\mathbf{P}^{-1} = \begin{bmatrix} -\mathbf{G}\mathbf{C}\mathbf{K}_c\mathbf{F} & -\mathbf{G}\mathbf{C}\mathbf{K}_c\mathbf{A} \\ -\mathbf{C}\mathbf{K}_c\mathbf{F} & -\mathbf{C}\mathbf{K}_c\mathbf{A} \end{bmatrix} = \boldsymbol{\Lambda}.$$

□

The following lemma gives conditions that guarantee that matrix $\boldsymbol{\Phi}$ is a convergent matrix.

Lemma 3
For any communication graph with at least one globally reachable vertex, the matrix $\boldsymbol{\Phi}$ defined in (27) is a convergent matrix.

Proof
Note that by making the partition

$$e^{\boldsymbol{\Lambda}h} = \begin{bmatrix} \mathbf{E}_{11} & \mathbf{E}_{12} \\ \mathbf{E}_{21} & \mathbf{E}_{22} \end{bmatrix},$$

with $\mathbf{E}_{11} \in \mathbb{R}^{(n-1)\times(n-1)}$, the matrix $\boldsymbol{\Phi}$ takes the simple form

$$\boldsymbol{\Phi} = \begin{bmatrix} \mathbf{E}_{11} & \mathbf{E}_{12} \\ 0 & 0 \end{bmatrix}. \tag{28}$$

Therefore, n of the eigenvalues of $\boldsymbol{\Phi}$ are zero while the remaining correspond to the eigenvalues of $\mathbf{E}_{11}$. Hence, the proof is reduced to showing that $\mathbf{E}_{11}$ is a convergent matrix.

First, a closed-form expression for $\mathbf{E}_{11}$ is derived using the fact that, by Lemma 2, $\boldsymbol{\Lambda}$ is similar to a diagonal matrix, thus making it easy to compute the matrix exponential

$$e^{\boldsymbol{\Lambda}h} = \mathbf{P}e^{\boldsymbol{\Delta}h}\mathbf{P}^{-1} = \mathbf{P}\begin{bmatrix} e^{-\mathbf{C}\mathbf{K}_c\mathbf{D}h} & \mathbf{0}_{n\times(n-1)} \\ \mathbf{0}_{(n-1)\times n} & \mathbf{I}_{n-1} \end{bmatrix}\mathbf{P}^{-1}.$$

The closed-form expression for $\mathbf{E}_{11}$ is therefore

$$\mathbf{E}_{11} = \mathbf{I}_{n-1} - \mathbf{G}\left(\mathbf{I}_n - e^{-\mathbf{C}\mathbf{K}_c\mathbf{D}h}\right)\mathbf{D}^{+}\mathbf{F}.$$

Next rewrite $\mathbf{E}_{11}$ as

$$\mathbf{E}_{11} = \mathbf{I}_{n-1} - \mathbf{G}\mathbf{Q}\mathbf{D}^{+}\mathbf{F}, \tag{29}$$

by defining $\mathbf{Q} := \mathbf{I}_n - e^{-\mathbf{C}\mathbf{K}_c\mathbf{D}h} = \mathrm{diag}[q_i]_{n\times n}$, where $q_i = 1 - e^{-c_i k_{ci} d_i h} \in [0,1)$. The spectrum of $\mathbf{E}_{11}$ is given by

$$\sigma(\mathbf{E}_{11}) = 1 - \sigma(\mathbf{G}\mathbf{Q}\mathbf{D}^{+}\mathbf{F}). \tag{30}$$

The spectrum of $\mathbf{G}\mathbf{Q}\mathbf{D}^{+}\mathbf{F}$ can alternatively be characterized as (see, e.g, [23])

$$\sigma(\mathbf{G}\mathbf{Q}\mathbf{D}^{+}\mathbf{F}) = \sigma(\mathbf{Q}\mathbf{D}^{+}\mathbf{F}\mathbf{G})\backslash\{0\} = \sigma(\mathbf{Q}\mathbf{D}^{+}\mathbf{L})\backslash\{0\}.$$

Let $\mathbf{X} = \mathbf{Q}\mathbf{D}^+\mathbf{L}$. This matrix can be viewed as the Laplacian of a weighted digraph where the weight of an arc $(i,j) \in \mathcal{E}$ is equal to $q_i d_i^+$. Applying Gerschgorin circle theorem (see, e.g., [23]) to matrix $\mathbf{X}$, we have that all its eigenvalues will be contained in the union of the Gerschgorin disks

$$\sigma(\mathbf{Q}\mathbf{D}^+\mathbf{L}) \subseteq \bigcup_{i=1}^{n} \overline{\mathcal{D}}(x_{ii}, r_i)$$

where $x_{ii} = q_i d_i^+ l_{ii} = q_i$ and

$$r_i = \sum_{\substack{j=1 \\ j\neq i}}^{n} |x_{ij}| = \sum_{\substack{j=1 \\ j\neq i}}^{n} q_i d_i^+ |l_{ij}| = q_i d_i^+ \sum_{\substack{j=1 \\ j\neq i}}^{n} |l_{ij}| = q_i \,.$$

All of the above disks are contained in the enclosing disk

$$\overline{\mathcal{D}}(x_{ii}, r_i) \subseteq \overline{\mathcal{D}}(q, q) \subseteq \mathcal{D}(1,1) \cup \{0\}$$

for all $1 \leq i \leq n$, where $q = \max_i q_i < 1$. Because the digraph associated to $\mathbf{L}$ has at least one globally reachable vertex, the same happens to the digraph associated to $\mathbf{X}$. As stated in Section 2.2, the Laplacian of a digraph with at least one globally reachable vertex has a simple eigenvalue at zero. Thus, $\mathbf{X}$ has a simple eigenvalue at zero. Therefore, $\sigma(\mathbf{G}\mathbf{Q}\mathbf{D}^+\mathbf{F}) \subseteq \mathcal{D}(1,1)$ and using (30) we conclude that $\sigma(\mathbf{E}_{11}) \subseteq \mathcal{D}(0,1)$. Thus, $\mathbf{E}_{11}$ is convergent. □

We are now ready to prove our main result.

Proof of Theorem 2
The time response of the impulsive system (23)-(24) is given by

$$\boldsymbol{x}_C(t) = e^{\boldsymbol{\Lambda}(t-t_k)}\boldsymbol{\Phi}^k \boldsymbol{x}_C(t_0) + \boldsymbol{g}_{\boldsymbol{\zeta}}(t) + \sum_{p=0}^{k-1} \boldsymbol{\Phi}^p \mathbf{V} \boldsymbol{g}_{\boldsymbol{\zeta}}(t_{k-p}) \tag{31}$$

for all $t \in [t_k, t_{k+1})$ and $k \geq 0$, where

$$\boldsymbol{g}_{\boldsymbol{\zeta}}(t) = \int_{t_{k(t)}}^{t} e^{\boldsymbol{\Lambda}(t-s)} \mathbf{B}\boldsymbol{\zeta}(s)\, \mathrm{d}s \tag{32}$$

for all $t \geq t_0$ and $k(t) = \left\lfloor \frac{t-t_0}{h} \right\rfloor$, and

$$\mathbf{V} := \begin{bmatrix} \mathbf{I}_{n-1} & 0 \\ 0 & 0 \end{bmatrix}.$$

Let $\rho = \frac{1}{2}\lambda_{\max}(\boldsymbol{\Lambda} + \boldsymbol{\Lambda}^\top)$ denote the log-norm of $\boldsymbol{\Lambda}$ (see, e.g., [24]) and $b = \|\mathbf{B}\|$ denote the induced Euclidean norm of $\mathbf{B}$. Then, the norm of (32) can be upper bounded by

$$\begin{aligned}
\|\boldsymbol{g}_{\boldsymbol{\zeta}}(t)\| &\leq \int_{t_k}^{t} \|e^{\boldsymbol{\Lambda}(t-s)}\| \|\mathbf{B}\| \|\boldsymbol{\zeta}(s)\|\, ds \leq b \int_{t_k}^{t} e^{\rho(t-s)} \|\boldsymbol{\zeta}(s)\|\, ds \\
&\leq b\|\boldsymbol{\zeta}\|_{[t_k,t]} \int_{t_k}^{t} e^{\rho(t-s)}\, ds = \frac{b}{\rho}\left(e^{\rho(t-t_k)} - 1\right) \|\boldsymbol{\zeta}\|_{[t_k,t]} \\
&\leq \frac{b}{\rho}\left(e^{\rho h} - 1\right) \|\boldsymbol{\zeta}\|_{[t_k,t]} \,.
\end{aligned}$$

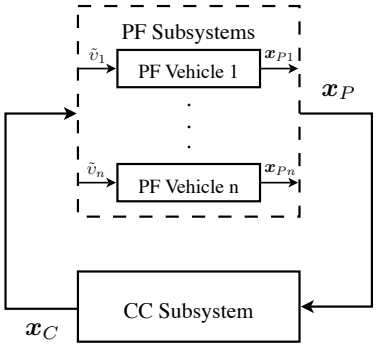

Figure 8. Interconnected system formed by n PF subsystems and the CC subsystem.

By Lemma 3, $\boldsymbol{\Phi}$ is a convergent matrix and therefore there exist $c_0 > 0$ and $\alpha < 1$ such that $\|\boldsymbol{\Phi}^p\| \leq c_0 \alpha^p$ for all $p \geq 0$. Hence, the terms depending on $\boldsymbol{\zeta}$ in (31) can be upper bounded by

$$\begin{aligned}
\|\boldsymbol{g}_{\boldsymbol{\zeta}}(t) + \sum_{p=0}^{k-1} \boldsymbol{\Phi}^p \mathbf{V} \boldsymbol{g}_{\boldsymbol{\zeta}}(t_{k-p})\| &\leq \|\boldsymbol{g}_{\boldsymbol{\zeta}}(t)\| + \sum_{p=0}^{k-1} \|\boldsymbol{\Phi}^p\| \|\mathbf{V}\| \|\boldsymbol{g}_{\boldsymbol{\zeta}}(t_{k-p})\| \\
&\leq \frac{b}{\rho}\left(e^{\rho h} - 1\right)\left(\|\boldsymbol{\zeta}\|_{[t_k,t]} + \sum_{p=0}^{k-1} c_0 \alpha^p \|\boldsymbol{\zeta}\|_{[t_{k-p-1},t_{k-p}]}\right) \\
&\leq \frac{b}{\rho}\left(e^{\rho h} - 1\right)\left(\|\boldsymbol{\zeta}\|_{[t_k,t]} + c_0 \|\boldsymbol{\zeta}\|_{[t_0,t_k]} \sum_{p=0}^{k-1} \alpha^p\right) \\
&\leq \frac{b}{\rho}\left(e^{\rho h} - 1\right)\left(1 + \frac{c_0}{1-\alpha}\right)\|\boldsymbol{\zeta}\|_{[t_0,t]},
\end{aligned}$$

where we used the fact that $\|\mathbf{V}\| = 1$, and that

$$\sum_{p=0}^{k-1} \alpha^p = \frac{1-\alpha^k}{1-\alpha} \leq \frac{1}{1-\alpha}, \text{ for } |\alpha| < 1\,.$$

Let

$$\sigma_C = \frac{b}{\rho}\left(e^{\rho h} - 1\right)\left(1 + \frac{c_0}{1-\alpha}\right). \tag{33}$$

Upper bounding the norm of (31), we conclude that

$$\|\boldsymbol{x}_C(t)\| \leq \kappa_C e^{-\lambda_C (t-t_0)} \|\boldsymbol{x}_C(t_0)\| + \sigma_C \|\boldsymbol{\zeta}\|_{[t_0,t]}\,.$$

for some positive constants κ_C and λ_C. □

3.5. System interconnection

The control structure proposed in Section 3.2, together with the control laws developed in Sections 3.3 and 3.4, form the interconnected system shown in Figure 8. The next theorem shows that the resulting interconnected controller solves the CPF problem presented in Section 2.3.

Theorem 3
The overall system formed by the interconnection of the n PF subsystems and the CC subsystem is globally asymptotically stable for an adequate choice of controller gains.

Proof
First, we show that the collection of PF subsystems is ISS with respect to state $\boldsymbol{x}_P := [\boldsymbol{x}_{P1}^\top \; \boldsymbol{x}_{P2}^\top \; \cdots \; \boldsymbol{x}_{Pn}^\top]^\top \in \mathbb{R}^{6n}$ and input $\boldsymbol{x}_C$. Let $\tilde{\boldsymbol{\upsilon}} := [\tilde{\upsilon}_i]_{n\times 1}$. We have that

$$\begin{aligned}
\|\boldsymbol{x}_P(t)\| &\leq \sum_{i=1}^{n} \|\boldsymbol{x}_{Pi}(t)\| \\
&\leq \sum_{i=1}^{n} \kappa_{Pi} e^{-\lambda_{Pi}(t-t_0)} \|\boldsymbol{x}_{Pi}(t_0)\| + \sigma_{Pi} \sup_{s\in[t_0,t]} |\tilde{\upsilon}_i(s)| \\
&\leq \Big(\sum_{i=1}^{n} \kappa_{Pi} e^{-\lambda_{Pi}(t-t_0)}\Big) \|\boldsymbol{x}_P(t_0)\| + \Big(\sum_{i=1}^{n} \sigma_{Pi}\Big) \sup_{s\in[t_0,t]} \|\tilde{\boldsymbol{\upsilon}}(s)\| \\
&\leq \kappa_P e^{-\lambda_P(t-t_0)} \|\boldsymbol{x}_P(t_0)\| + \sigma_P \sup_{s\in[t_0,t]} \|\tilde{\boldsymbol{\upsilon}}(s)\|
\end{aligned}$$

where $\kappa_P = \sum_{i=1}^{n} \kappa_{Pi}$, $\lambda_P = \min_{1\leq i\leq n} \lambda_{Pi}$, and $\sigma_P = \sum_{i=1}^{n} \sigma_{Pi}$. Moreover, $\tilde{\boldsymbol{\upsilon}}$ and $\boldsymbol{x}_C$ are related as follows

$$\begin{aligned}
\tilde{\boldsymbol{\upsilon}} &= -\mathbf{K}_c \mathbf{D} \boldsymbol{\chi} + \mathbf{K}_c \mathbf{A} \hat{\boldsymbol{\chi}} \\
&= -\mathbf{K}_c \mathbf{F} \boldsymbol{\theta} - \mathbf{K}_c \mathbf{A} \tilde{\boldsymbol{\chi}} \\
&= -\mathbf{K}_c \begin{bmatrix} \mathbf{F} & \mathbf{A} \end{bmatrix} \boldsymbol{x}_C .
\end{aligned}$$

Using the bound

$$\|\tilde{\boldsymbol{\upsilon}}\| \leq \sigma_{\max}\big(\mathbf{K}_c \begin{bmatrix} \mathbf{F} & \mathbf{A} \end{bmatrix}\big) \|\boldsymbol{x}_C\|,$$

yields

$$\|\boldsymbol{x}_P(t)\| \leq \kappa_P e^{-\lambda_P(t-t_0)} \|\boldsymbol{x}_P(t_0)\| + \tilde{\sigma}_P \|\boldsymbol{x}_C\|_{[t_0,t]}$$

where $\tilde{\sigma}_P = \sigma_{\max}\big(\mathbf{K}_c \begin{bmatrix} \mathbf{F} & \mathbf{A} \end{bmatrix}\big) \sigma_P$.

Next, we show that the CC subsystem is ISS with respect to state $\boldsymbol{x}_C$ and input $\boldsymbol{x}_P$. From Theorem 2, we know that

$$\|\boldsymbol{x}_C(t)\| \leq \kappa_C e^{-\lambda_C(t-t_0)} \|\boldsymbol{x}_C(t_0)\| + \sigma_C \|\boldsymbol{\zeta}\|_{[t_0,t]}.$$

Resorting to the following bounds

$$\|\zeta_i\| \leq w_i \beta_{1i} \|\boldsymbol{z}_{1i}\| \leq w_i \beta_{1i} \|\boldsymbol{x}_{Pi}\| \Rightarrow \|\boldsymbol{\zeta}\| \leq \bar{w}\bar{\beta}_1 \|\boldsymbol{x}_P\|$$

where $\bar{w} = \max_{1\leq i\leq n} w_i$ and $\bar{\beta}_1 = \max_{1\leq i\leq n} \beta_{1i}$, we conclude that

$$\|\boldsymbol{x}_C(t)\| \leq \kappa_C e^{-\lambda_C(t-t_0)} \|\boldsymbol{x}_C(t_0)\| + \tilde{\sigma}_C \|\boldsymbol{x}_P\|_{[t_0,t]}$$

where $\tilde{\sigma}_C = \bar{w}\bar{\beta}_1 \sigma_C$.

Applying a small-gain theorem (Theorem 1) to the collection of PF subsystems to the CC subsystem, we get that a sufficient condition for asymptotical stability of the interconnected system is

$$\tilde{\sigma}_P \tilde{\sigma}_C < 1 \,. \tag{34}$$

Since σ_P can be made arbitrary small by increasing the PF gains ($\mathbf{K}_1$ and $\mathbf{K}_2$), this condition can always be satisfied. □

Remark
The reason why we choose to increase the PF gains $\mathbf{K}_1$ and $\mathbf{K}_2$ in the proof of Theorem 3 instead of decreasing h, is that $\tilde{\sigma}_C$ cannot be made arbitrarily small by decreasing h, since σ_C in (33) as a function of h has a minimum value. Therefore, if the PF gains are fixed, asymptotical stability may not be possible to guarantee using the reasoning of Theorem 3.

Table I. Physical parameters of the vessels.

Type of parameter	Symbol	Vessel 1	Vessel 2	Vessel 3	Units
Mass*	m_u	500	515	485	kg
	m_v	1000	990	1010	kg
Moment of inertia*	I_r	700	735	700	$\mathrm{kg\,m^2}$
Hydrodynamic damping	X_u	−1	−1.1	−0.9	$\mathrm{kg\,s^{-1}}$
	$X_{\lvert u\rvert u}$	−25	−22.5	−27.5	$\mathrm{kg\,m^{-1}}$
	Y_v	−10	−9	−11	$\mathrm{kg\,s^{-1}}$
	$Y_{\lvert v\rvert v}$	−200	−220	−180	$\mathrm{kg\,m^{-1}}$
	N_r	−0.5	−0.45	−0.55	$\mathrm{kg\,m^2\,s^{-1}}$
	$N_{\lvert r\rvert r}$	−1500	−1650	−1350	$\mathrm{kg\,m^2}$

*added mass terms included.

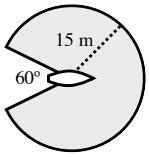

Figure 9. Communication range for each vessel: every other vessel inside the gray area will receive data.

4. ILLUSTRATIVE EXAMPLE

We consider a group of three ASVs whose kinematic and dynamic equations of motion can be written as in (1)-(3), with

$$\mathbf{M} = \mathrm{diag}(m_u, m_v, I_r), \text{ and } \boldsymbol{f}(\boldsymbol{\eta}, \boldsymbol{\nu}) = \begin{bmatrix} X_u + X_{|u|u}|u| & -m_v r & 0 \\ m_u r & Y_v + Y_{|v|v}|v| & 0 \\ 0 & 0 & N_r + N_{|r|r}|r| \end{bmatrix} \boldsymbol{\nu}\,.$$

In the simulations presented, the physical parameters are given in Table I. The communication range of each vessel is the circular sector illustrated in Figure 9.

The initial time is $t_0 = 0\,\mathrm{s}$ and the simulation is run for $T_{\mathrm{sim}} = 200\,\mathrm{s}$. The initial conditions of each vessel are $\boldsymbol{\eta}_1(t_0) = (5\,\mathrm{m}, 20\,\mathrm{m}, \pi/3\,\mathrm{rad})$, $\boldsymbol{\eta}_2(t_0) = (-10\,\mathrm{m}, 10\,\mathrm{m}, -\pi/4\,\mathrm{rad})$, $\boldsymbol{\eta}_3(t_0) = (0\,\mathrm{m}, -15\,\mathrm{m}, -2\pi/3\,\mathrm{rad})$, $u_i(t_0) = v_i(t_0) = 0\,\mathrm{m\,s^{-1}}$ and $r_i(t_0) = 0\,\mathrm{rad\,s^{-1}}$ for $i = 1, 2, 3$. The initial condition for $\boldsymbol{\gamma}$ is chosen so that for vessel i, γ_i yields the closest point on the corresponding path, which gives $\boldsymbol{\gamma}(t_0) = (5, -10, 0)\,[\mathrm{m}]$. The reference speed is set to $v_{\mathcal{L}} = 1\,\mathrm{s^{-1}}$. A scaling is performed during the arcs to ensure that all the vessels reach the second set of straight lines at the same time. This is done by setting $R_{1,3} = \frac{\pi}{2}$ and $R_2 = 1$ during that section of the path ($R_i = 1$ everywhere else).

The PF gains are the same for all vessels: $\mathbf{K}_1 = 40\mathbf{I}_3$ and $\mathbf{K}_2 = 200\mathbf{I}_3$. The CC gains are $\mathbf{K}_c = 0.79\mathbf{D}^{+}\mathbf{C}^{-1}$ and $\mathbf{W} = 10^{-3}\mathbf{C}^{-1}$, where the entries of $\mathbf{C}$ depend on whether the vehicle is moving along a straight line or a circumference's arc. The gains were selected in order to verify condition (34) over all possible network topologies that have a globally reachable vertex and with a communication period of $h = 1\,\mathrm{s}$.

Figure 10 illustrates the trajectories made by the vessels. The vessels start by converging to a set of straight lines 25 m from each other. As we will see, this disconnects the vessels from one another. They are then brought closer together along straight lines that are 5 m apart. Along these straight lines, first an "inline" formation pattern characterized by $\boldsymbol{\phi}_0 = (0, 0, 0)$ is acquired. At $t = t_{\phi 1} = 70\,\mathrm{s}$, the formation pattern is changed into the "slanted" configuration represented by $\boldsymbol{\phi}_1 = (10, 0, -10)$. At $t = t_{\phi 2} = 110\,\mathrm{s}$, the vessels return to the original inline pattern and at $t = t_{\phi 3} = 140\,\mathrm{s}$ the pattern changes into a mirrored version of the slanted formation ($\boldsymbol{\phi}_3 = (-10, 0, 10)$).

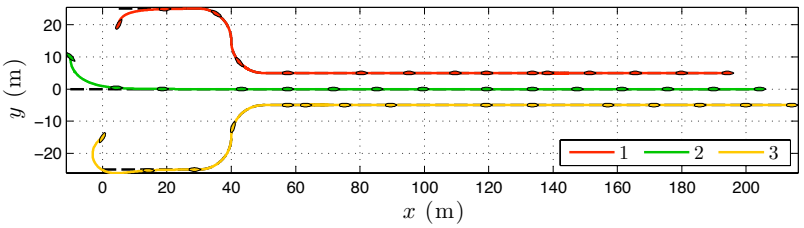

Figure 10. Trajectory of each vessel in the 2D-plane.

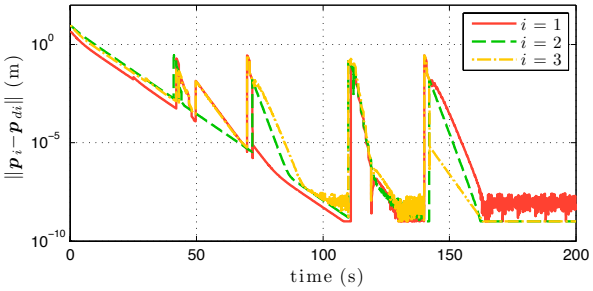

Figure 11. Time evolution of the path-following position errors.

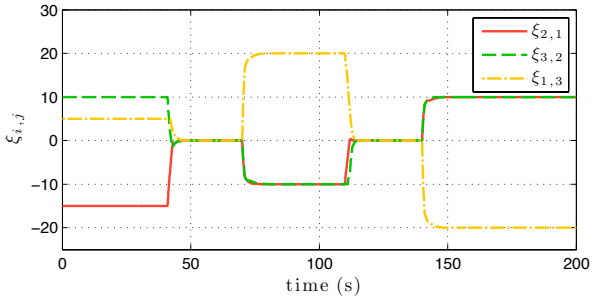

Figure 12. Time evolution of the along-path distances.

Figure 11 shows the time evolution of the position errors of each vessel, given by $\|\boldsymbol{p}_i(t) - \boldsymbol{p}_{di}(\gamma_i(t))\|$, where $\boldsymbol{p}_i(t) = (x_i(t), y_i(t))$ and $\boldsymbol{p}_{di}(t) = (x_{di}(\gamma_i(t)), y_{di}(\gamma_i(t)))$. The peaks at $t = t_{\phi i}$ are due to changes in the spatial configuration, while others spikes stem from the fact that the path is not differentiable when changing from straight line to arcs and vice-versa. Figure 12 presents the time evolution of the along-path distances. As can be seen, the evolution of $\xi_{i,j}$ agrees with the initial inline formation $\boldsymbol{\phi}_0$ and after $t = t_{\phi 1}$ changes into the leader-following formation defined by $\boldsymbol{\phi}_1$, returning to the original pattern after $t = t_{\phi 2}$.

Due to the way the paths are designed, as well as the changes in formation patterns, the network graph changes over time. The time evolution of the network links is illustrated in Figure 13. Several network topologies are present and only some of them have at least one globally reachable vertex.

Although the gains are designed to ensure stability for $h = 1\,\mathrm{s}$, simulations were carried out at higher communication periods. Let $\boldsymbol{x}_{cl} = [\boldsymbol{x}_P^\top \; \boldsymbol{x}_C^\top]^\top$ denote the state of interconnected system shown in Figure 8. Figure 14 depicts the time evolution of its norm. During time intervals where connectivity is preserved the system remains stable with errors converging to zero, and in the absence of connectivity the vessels will do cooperation in smaller groups

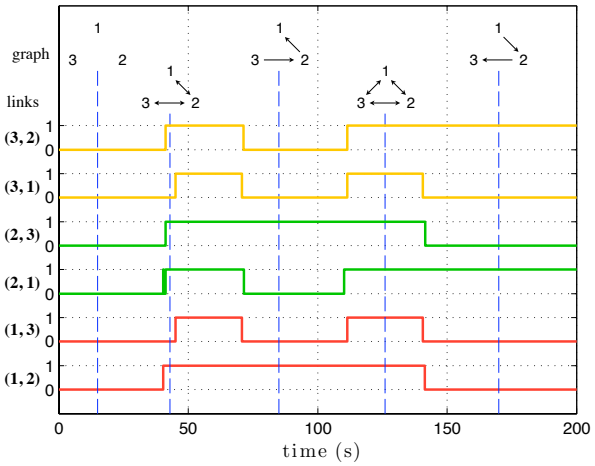

Figure 13. Time evolution of the links between vessels and snapshots of the underlying graph at certain time instants. Arrows signal flow of information.

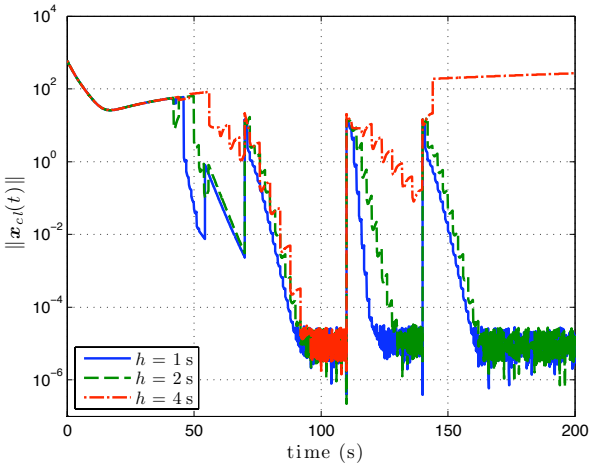

Figure 14. Time evolution of the closed-loop state's norm for different values of h without any input saturation.

and/or path-following as if the other vessels did not exist. Figure 14 also shows that during time intervals where connectivity exists, the rate of convergence decreases when h increases.

To assess the effect of saturation of the control input in the overall performance of the closed-loop system, we performed simulations where the propulsion system of each vessel has the following limitations: given $\tau_{\max} \geq 0$,

$$|\tau_{ui}| \leq \tau_{\max}(\mathrm{N}) \quad |\tau_{vi}| \leq \frac{1}{5}\tau_{\max}(\mathrm{N}) \quad |\tau_{ri}| \leq 3\tau_{\max}(\mathrm{Nm})$$

for $i = 1, 2, 3$. To measure the variation in performance, let the root mean squared (RMS) value of $\boldsymbol{x}_{cl}$ be defined as

$$\mathrm{RMS}\{\boldsymbol{x}_{cl}\} = \sqrt{\frac{1}{T_{\mathrm{sim}} - t_0} \int_{t_0}^{T_{\mathrm{sim}}} \boldsymbol{x}_{cl}^{\top}(t)\boldsymbol{x}_{cl}(t)\,\mathrm{d}t},$$

and let T_{conn} denote the total amount of time where there is at least one globally reachable vertex in the induced communication graph. Plotted in Figure 15 are the values of RMS and

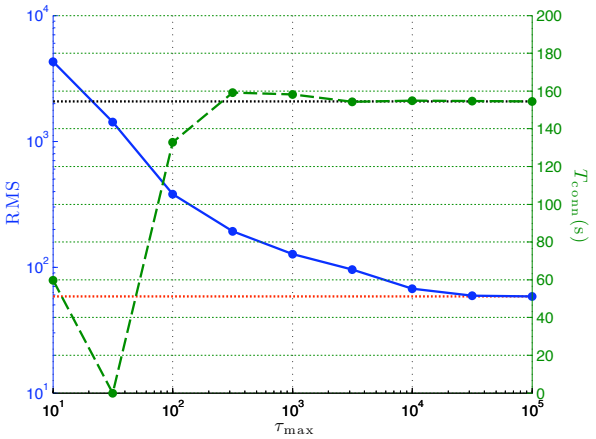

Figure 15. Variation of RMS$\{\boldsymbol{x}_{cl}\}$ and T_{conn} for different values of $\tau_{\max}$ with communication period $h = 1\,\text{s}$. The red and black dotted lines represent the RMS and T_{conn} values obtained without saturation.

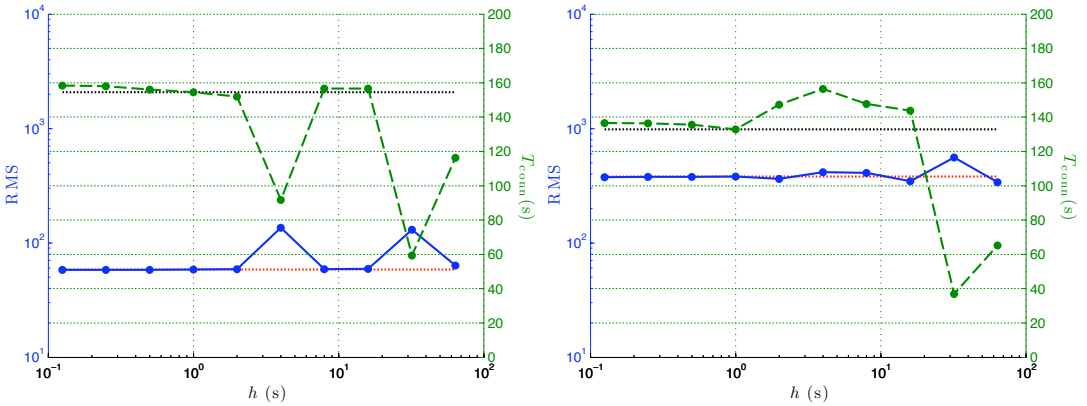

(a) $\tau_{\max} = \infty$. (b) $\tau_{\max} = 100$.

Figure 16. Variation of RMS$\{\boldsymbol{x}_{cl}\}$ and T_{conn} for different values of the communication period h and two different values of input saturation. The red and black dotted lines represent the RMS and T_{conn} values obtained with $h = 1\,\text{s}$ in each case.

T_{conn} for different values of $\tau_{\max}$. As expected, when $\tau_{\max}$ decreases, performance worsens and connectivity is kept for less and less time. For $\tau_{\max} = 10^2$ the performance is quite degraded but T_{conn} is only slightly less than the one obtained without any saturation in the inputs, showing that some degree of saturation is well tolerated. When $\tau_{\max}$ goes below 10^2, the propulsion system is so limited that the vehicles cannot perform the required path-following maneuvers. When this happens, performance and connectivity cannot be increased by decreasing the communication period h.

As before, we now compare the variation in performance and connectivity with a fixed saturation limit $\tau_{\max}$ and varying communication period h. Shown in Figure 16(a)-(b) are the values of RMS and T_{conn} for different values of h when there is no input saturation and when $\tau_{\max} = 100$, respectively. Decreasing the communication period h does not affect RMS performance or total connectivity time significantly, but its increase eventually leads to a loss of connectivity (that is, a decrease of T_{conn}).

5. CONCLUSION

We addressed the problem of cooperative path-following for a group of fully-actuated surface vessels that exchange messages among each other at periodic intervals. Each vessel must follow a pre-assigned path while keeping a desired spatial configuration relative to the other vessels. Lyapunov and model-based control techniques together with concepts from graph theory are employed to characterize the stability properties of the proposed decentralized control structure formed by an interconnection of two subsystems: path-following and cooperation control. Both subsystems are shown to be input-to-state stable with respect to each other, and therefore, resorting to a small-gain theorem, asymptotical stability of the overall system is guaranteed for large enough path-following controller gains, as long as the graph induced by the communication network has at least one globally reachable vertex. An illustrative example with extensive simulation results performed under limited communication range, varying network topologies, and actuator saturation show that the proposed control system tolerates well nonlinear effects not taken into account during the design phase.

ACKNOWLEDGEMENTS

This work is partially supported by the FREEsubNET Research Training Network of the European Union under contract number MRTN-CT-2006-036186, the European Commission through the TRIDENT project under contract number FP7-ICT2009-248497, project Co3AUVs/CEC under grant number IST-231378, and the FCT-ISR/IST plurianual funding program (through the POS-Conhecimento Program initiative in cooperation with FEDER).

The work of J. Almeida was supported by grant number SFRH/BD/30605/2006 from Fundação para a Ciência e a Tecnologia (FCT).

REFERENCES

1. Schoenwald DA. Auvs: In space, air, water, and on the ground. *IEEE Control Systems Magazine* Dec 2000; **20**(6):15–18.
2. Gomes P, Silvestre C, Pascoal A, Cunha R. A coast line following preview controller for the DELFIMx vehicle. *Proc. of the 17th International Offshore and Polar Engineering Conference and Exhibition*, Lisbon, Portugal, 2007.
3. Pascoal A, Oliveira P, Silvestre C, Sebastião L, Rufino M, Barroso V, Gomes JP, Ayela G, Coince P, Cardew M, *et al.*. Robotic ocean vehicles for marine science applications: the european ASIMOV project. *Proc. of OCEANS 2000 MTS/IEEE*, Providence, Rhode Island, USA, 2000; 409–415.
4. Aguiar A, Almeida J, Bayat M, Cardeira B, Cunha R, Häusler A, Maurya P, Oliveira A, Pascoal A, Pereira A, *et al.*. Cooperative autonomous marine vehicle motion control in the scope of the EU GREX project: Theory and practice. *Proc. of OCEANS 2009 MTS/IEEE*, Bremen, Germany, 2009.
5. Arrichiello F, Chiaverini S, Fossen TI. *Group Coordination and Cooperative Control*, *Lecture Notes in Control and Information Systems*, vol. 336, chap. Formation Control of Marine Surface Vessels using the Null-Space-Based Behavioral Control. Springer-Verlag, 2006.
6. Ihle IA, Jouffroy J, Fossen TI. *Group Coordination and Cooperative Control*, *Lecture Notes in Control and Information Systems*, vol. 336, chap. Robust Formation Control of Marine Craft using Lagrange Multipliers. Springer-Verlag, 2006.
7. Murray RM. Recent research in cooperative control of multivehicle systems. *Journal of Dynamic Systems, Measurement and Control* Sep 2007; **129**(5):571–583.
8. Børhaug E, Pavlov A, Pettersen KY. Straight line path following for formations of underactuated underwater vehicles. *Proc. of the 46th Conf. on Decision and Control*, New Orleans, LA, USA, 2007; 2905–2912.
9. Zhang F, Frantantoni DM, Paley DA, Lund JM, Leonard NE. Control of coordinated patterns for ocean sampling. *Int. J. of Control* Jul 2007; **80**(7):1186–1199.
10. Ghabcheloo R, Aguiar AP, Pascoal A, Silvestre C, Kaminer I, Hespanha JP. Coordinated path-following of multiple underactuated autonomous vehicles in the presence of communication failures. *Proc. of the 45th Conf. on Decision and Control*, San Diego, CA, USA, 2006; 4345–4350.
11. Ghabcheloo R, Pascoal A, Silvestre C, Kaminer I. Nonlinear coordinated path following control of multiple wheeled robots with bidirectional communication constraints. *Int. J. of Adaptive Control and Signal Processing* Oct 2007; **21**(2-3):133–157.
12. Ihle IAF, Arcak M, Fossen TI. Passivity-based designs for synchronized path-following. *Automatica* Sep 2007; **43**(9):1508–1518.
13. Encarnação P, Pascoal A. Combined trajectory tracking and path following for marine craft. *9th Mediterranean Conf. on Control and Automation*, Dubrovnik, Croatia, 2001.

14. Skjetne R, Fossen TI, Kokotović PV. Adaptive output maneuvering with experiments for a model ship in a marine control laboratory. *Automatica* Nov 2005; **41**(4):289–298.
15. Montestruque LA, Antsaklis PJ. On the model-based control of networked systems. *Automatica* Oct 2003; **39**(10):1837–1843.
16. Godsil C, Royle G. *Algebraic Graph Theory*. Graduate Texts in Mathematics, Springer-Verlag New York, Inc, 2001.
17. Fossen T. *Guidance and control of ocean vehicles*. John Wiley & Sons, Inc.: New York, USA, 1994.
18. Lin Z, Francis B, Maggiore M. Necessary and sufficient conditions for formation control of unicycles. *IEEE Transactions on Automatic Control* Jan 2005; **50**(1):121–127.
19. Olfati-Saber R, Murray RM. Consensus problems in networks of agents with switching topology and time-delays. *IEEE Transactions on Automatic Control* Sep 2004; **49**(9):1520–1533.
20. Isidori A. *Nonlinear Control Systems II*. Springer-Verlag: London, 1999.
21. Khalil HK. *Nonlinear Systems*. Prentice Hall: Upper Saddle River, New Jersey, USA, 2002.
22. Krstić M, Kanellakopoulos I, Kokotović P. *Nonlinear and Adaptive Control Design*. John Wiley & Sons, Inc.: New York, USA, 1995.
23. Horn RA, Johnson CR. *Matrix Analysis*. Cambridge University Press: New York, NY, USA, 1990.
24. Van Loan C. The sensitivity of the matrix exponential. *SIAM Journal on Numerical Analysis* Dec 1977; **14**(6):971–981.